Wiley
International Transactions on Electrical Energy Systems
Volume 2024, Article ID 5546037, 17 pages
https://doi.org/10.1155/etep/5546037

WILEY

Research Article

A Charger Current–Limiting Scheme to Improve Protection Coordination of Electric Vehicle–Integrated Distribution Systems

Majid Tavoosi[1], **Bahador Fani**[1], **Majid Delshad**[1] and **Iman Sadeghkhani**[2,3]

[1]*Department of Electrical Engineering, Isfahan (Khorasgan) Branch, Islamic Azad University, Isfahan, Iran*
[2]*Smart Microgrid Research Center, Najafabad Branch, Islamic Azad University, Najafabad, Iran*
[3]*Department of Electrical Engineering, Najafabad Branch, Islamic Azad University, Najafabad, Iran*

Correspondence should be addressed to Bahador Fani; bahadorfani@gmail.com

Received 16 March 2024; Revised 26 July 2024; Accepted 28 October 2024

Academic Editor: Santi A. Rizzo

Although the development of electric vehicle (EV) technology offers opportunities for reducing CO_2 emissions through the electrification of transportation, the integration of EVs into distribution systems poses a significant challenge to the reliable operation of existing protection systems. As the penetration level of EVs continues to rise, the fault current characteristic of the distribution system changes, resulting in load de-energization, equipment damage, and reduced reliability. This paper develops a protection scheme for preserving coordination between main and backup overcurrent relays considering various penetration levels and locations of integrated EVs. By modifying the EV charger control system, the proposed scheme limits the fault current contribution of adopted EV charge stations into the fault point. The developed scheme does not alter the structure of the available protection system of the distribution network and is compatible with both old and nonprogrammable relays. Furthermore, it does not require communication links. The effectiveness of the proposed scheme is validated through several case studies on the Isfahan distribution network. The findings indicate that the operating time of the backup relay in the conventional protection system exceeds the thermal limit at 100% penetration level of EVs installed upstream of this relay as it reaches 1810 ms, while by using the proposed strategy, this time reduces to 776 ms, preserving protection coordination between the main and backup relays.

Keywords: charger controller; distribution system; electric vehicle; overcurrent relay; protection coordination

1. Introduction

1.1. Research Motivation. Electric vehicles (EVs) are essential for addressing energy resource limitations and decarbonizing road transport, comprising over 15% of global energy emissions. It significantly increases the investment in EV technology and charging infrastructure, with a 54% increase reported in 2022 [1, 2]. The leading EV markets are the United States, Europe, and China. Recent growth suggests potential alignment with the net zero emissions' scenario by 2030. Conventionally, the primary purpose of grid integration of EVs is to charge their batteries. However, in today's and future smart grids, EV charging stations (EVCSs) can serve an additional function by supplying power back to the grid. This capability enables EVCSs to contribute to the balancing of electricity generation from renewable energy sources in the grid, as well as supporting grid operations through the charge/discharge capability of EV batteries, which can include providing ancillary services such as harmonic mitigation, reactive power supply, and peak power shaving through vehicle-to-grid (V2G) schemes [3–6]. The evolution of EVCSs from simple load points to bidirectional energy interfaces with the grid represents a significant opportunity for enhancing grid flexibility and resilience, while also maximizing the benefits of renewable energy integration.

The widespread integration of EVs into the distribution network profoundly affects both the operational modes and the structural configuration of the system, as well as the distortion patterns of electrical parameters during faults in

electrical feeders [7, 8]. With higher levels of EV integration, conventional protection devices (PDs) such as overcurrent relays (OCRs) face new challenges, potentially jeopardizing their effective coordination [9]. The impact of EV grid integration during a fault condition differs markedly from normal operations, potentially leading to the malfunction of the protection system. Such disruptions can alter the short-circuit level and direction of fault currents, inadvertently causing circuit breakers (CBs) to trip [10, 11]. Therefore, the task of setting protection and maintaining coordination between different protection zones has grown increasingly complex. This complexity underscores the tension among the four principal demands of relay protection: reliability, selectivity, speed, and sensitivity. This situation calls for a comprehensive reevaluation of the distribution system's protection mechanisms in light of EV integration.

1.2. Literature Review. The available protection schemes mainly comprise two main strategies to enhance the performance of the protection system in the presence of active power sources (APSs). The first strategy is related to preserving the available conventional protection, which includes disconnection of APSs, limiting penetration level, and using a fault current limiter (FCL) to prevent significant changes in the network current profile [12–14]. Disconnection of APSs' controllers increases the probability of damage to chargers and the reliance on the protection validity of detection methods, thus reducing reliability. Limiting penetration level-based schemes take into account some factors such as harmonic constraints, voltage constraints, and protection adaptability and passively determine the permissible penetration level of APSs in the distribution system; however, it deprives the distribution system of services of APSs in normal operation. The FCL is costly and its impedance is difficult to determine. Another conventional practice involves optimizing the capacity and location of distributed APSs without revising the existing PDs. Computational algorithms in [15–17] are used to identify the optimal location and size of distributed APSs to address the protection miscoordination problem. This approach could be technically and economically efficient compared to FCL-based techniques due to its high initial cost [18]. Generally, in addition to their complexity, these schemes limit the possible locations of distributed resources. Furthermore, the performance of these schemes may deteriorate when the network topology changes.

By modifying the protection system design through changes in protection hardware [19–21], adaptive protection schemes [22–30], and fault locating techniques based on communication technology [31, 32], the second category of schemes aims to ensure the proper operation of the PDs. The use of new and programmable relays, distance relays, differential relays, and directional OCRs is proposed in [19–21]. However, this scheme is significantly costly for the distribution utility companies, usually resulting in complex protection settings and requiring the updating of the scheme in the case of network topology changes. Adaptive protection approaches work with existing protection setups, dynamically adjusting settings based on real-time calculations of network parameters to identify and isolate faults [22–26]. The authors in references [27–30] enhance coordination through multiagent systems and communication networks among PDs, offering precision and efficiency but at the expense of higher costs and potential reliability issues due to communication breakdowns. Fault location leverages data analysis of electrical measurements [31, 32], which becomes challenging with the dynamic nature of networks integrating APSs, especially with the rising integration of EVs, necessitating new adaptable protection schemes [33, 34].

There are few studies conducted on the impact of EVCSs on the relay protection of power distribution networks. In [35], the operational mechanism of EVCSs is described in relation to charging load characteristics and its influence on the overcurrent protection of power distribution lines. In addition, an overcurrent protection scheme based on the reactive power error component is presented. The authors in reference [11] enhance the sensitivity of backup PDs of distribution networks by utilizing low-voltage overcurrent protection in the presence of EV charging stations. A fault detection scheme is developed in [36] where the frequency and voltage are directly measured, eliminating the need for a communication signal to protect the microgrid. It is designed to ensure the proper functioning of relays, particularly in islanded conditions and communication infrastructure outages, by controlling the operation of integrated EVs to inject high current into the microgrid and establishing the required fault current threshold. This adaptive protection scheme is effective even in the event of a cyber-attack that compromises the communication platform. The authors in references [37, 38] develop protection schemes for EVCSs where they are disconnected during a fault condition. Due to the increasing popularity of DC fast chargers, these protection plans are primarily based on calculations and fault analysis at the DC bus level.

1.3. Necessity of the Research. To the best of our knowledge, the impact of EV integration levels and locations on distribution network protection systems has not been adequately addressed. Addressing the challenge of maintaining selectivity and sensitivity in protection within EV-enhanced distribution networks, this paper introduces a scheme that ensures the coordination of existing protection systems for various EV integration scenarios. The scheme, which modifies the EV charger control system to manage fault current contributions, identifies specific EVCSs that significantly influence the protection system and limits their output to preserve coordination without recurrent adjustments. This strategy does not rely on communication links and keeps the current protection system configuration intact, even with older, nonprogrammable relays. Table 1 compares the proposed scheme with some existing ones on EV's impact on distribution system protection.

1.4. Main Contributions. Specifically, the main contributions of this paper are as follows:

Table 1: Comparison of the proposed protection scheme with some existing schemes on EV's impact on distribution system protection.

	[35]	[11]	[36]	[37]	[38]	Proposed scheme
Independence from penetration levels and location of EVs	X	X	X	X	X	✓
No need to replace or add a protective device	✓	✓	X	✓	X	✓
No need for online compatibility	X	X	X	✓	✓	✓
High penetration level of EV integration	X	X	X	X	✓	✓
High-impedance fault simulation	X	X	X	✓	✓	✓
No need for the communication link	✓	✓	✓	✓	X	✓
Network topology change consideration	X	X	✓	X	✓	✓
Sensitivity analysis of protective device	X	X	X	X	X	✓
No need to use new programmable relays	✓	✓	✓	X	X	✓

- EV's impact on fault current and performance of the protection scheme is evaluated at various penetration levels and locations within the distribution network.
- The proposed scheme is independent of the penetration level and location of EVs.
- The proposed scheme is offline and communication-free.
- The proposed scheme is compatible with both conventional and programmable relays.
- Additional investment such as protective device replacement and installations and online control function design are not required when using the proposed scheme.

1.5. Paper Structure. The paper's structure is as follows. Section 2 examines the impact of high EV integration levels on feeder protection systems. Section 3 identifies scenarios leading to coordination loss and offers a solution for its restoration. Section 4 presents the proposed charger current limiting (CCL)–based protection scheme. Section 5 presents simulation case studies to demonstrate the scheme's effectiveness, followed by a sensitivity analysis in Section 6. Finally, Section 7 concludes the findings.

2. Impact of EV Integration on Protection System

The growing EV market results in a large number of EVCSs, which serve as the interfaces for EV grid integration. Potentially, during different hours of the day, due to variations in integration time, geographical distribution, and charging patterns, there are various penetration levels of EV grid integration [4, 6]. The penetration level of EVs in the charging state in a feeder is defined as

$$\text{penetration level}\,(\%) = \frac{\sum_{j=1}^{m} P_{\text{EV}_j}}{\sum_{k=1}^{l} P_{\text{other load}_k}} \times 100, \qquad (1)$$

where P_{EV} and $P_{\text{other loads}}$ are the stored real power of integrated EVs and the real power of the other loads of the network, respectively. m and l are the number of integrated EVs and network loads, respectively. To consider the EVCS integration into the distribution system, the available capacity for connecting other loads is reduced. This means that the total capacity of both EVCS and other connected loads should not exceed the permissible capacity of the distribution transformer at each bus. Therefore, the penetration level of EVCS is defined based on this limitation to ensure that the current on the main distribution feeder does not exceed its thermal limit. In this study, under worst-case conditions, it is assumed that the maximum rating of EVCS at a bus is equal to that of other loads. Typically, in distribution feeder protection settings, relay adjustments are made based on the relay current during faults, meaning any variation in this current could either disrupt or enhance relay performance under specific scenarios.

In distribution feeders, electricity flows from the upstream network to consumers located in downstream feeders. The level and location of integrated EVs dictate the current injected from the upstream network. When a fault occurs, sources of fault current include both the upstream network and EV batteries. The protection relay's current magnitude is influenced by the placement of EVCSs along the feeder, with the impedance between the upstream grid and the fault point determining the fault current's magnitude. With EV integration into the distribution system's feeders, relay currents in the downstream network near the EVCSs may significantly drop compared to those in the upstream network, potentially compromising the protection system's effectiveness due to reduced sensitivity, leading to nonoperation. Integrating EVs downstream of the main protection relay typically does not affect the protection system's operation. However, integrating EVs between the downstream and upstream relays, serving as main and backup protections, may result in losing coordination between them. In addition, integrating EVs upstream of the backup protection alters the current through both main and backup relays, which can, under certain circumstances, disrupt protection coordination.

Figure 1 shows a radial distribution system where both the backup relay OCR1 and the main relay OCR2 are conventional OCRs. When no EV is integrated into the distribution system, the main and backup relays coordinate their operation with an appropriate coordination time interval (CTI) for the short-circuit current I_g, as shown in Figure 2. To assess the protection coordination, the most critical cases, that is, the minimum and maximum fault currents through the main and backup relays, $I_F^{\min}$ and $I_F^{\max}$, respectively, are considered. These currents determine the operating times of the relays. In the conventional protection

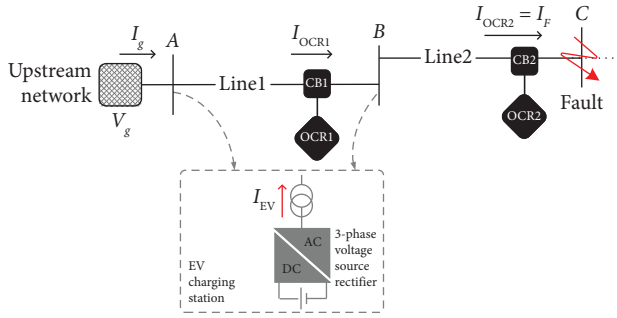

FIGURE 1: Schematic diagram of a radial distribution feeder in the presence of EVCSs.

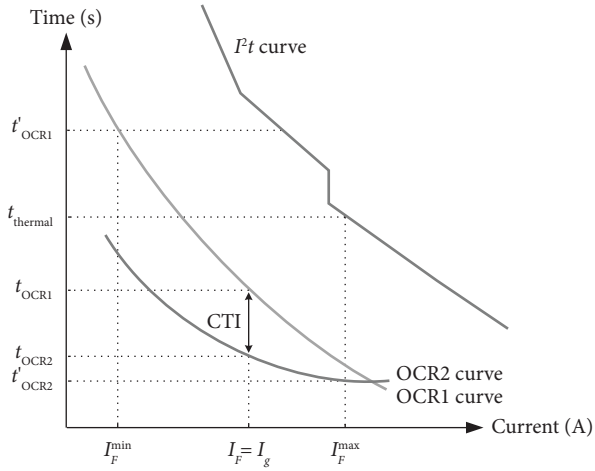

FIGURE 2: Characteristic curves of the main and backup protection relays from the paper [39] by Fani, Bisheh, and Sadeghkhani.

system, OCR1 and OCR2 correctly operate in the possible fault current range $[I_F^{min} I_F^{max}]$, maintaining a suitable CTI along their operational curves.

When EVs are integrated upstream from both main and backup relays and a fault occurs at the bus C in Figure 1, the current through OCR1 and OCR2 decreases compared to the case of no EV. A higher penetration level of integrated EVs further diminishes the current through these protection relays, consequently extending their activation times according to their respective characteristic curves. Should the diminished current fall within the range of $[I_F^{min} I_F^{max}]$, the inclusion of EVs can enhance protection coordination by ensuring an adequate operational window for the backup relay's activation time. Nonetheless, at a specific threshold of EV integration, the resultant current through OCR1 and OCR2 may drop below the minimum acceptable limit I_F^{min}. Under such circumstances, OCR1's response time exceeds the thermal tolerance of the network's conductive materials. The resultant elevated current during fault conditions can potentially escalate conductor temperatures, risking damage to the network infrastructure. This scenario is regulated by the IEC 60909 standard [40], which stipulates the thermal threshold for conductors as

$$I^2 t \leq K^2 S^2, \tag{2}$$

where I is the root mean square (RMS) value of the fault current in amperes, t is the fault duration (clearing) time in seconds, and S denotes the cross-sectional area of the conductor in square millimeters. K is a coefficient determined by the type of conductor material. According to this standard, the maximum duration for clearing a fault must not exceed the conductor's thermal limit. To adhere to this guideline, the operational curves of the protection system must lie beneath the thermal limit curve (the I^2t curve) as illustrated in Figure 2. When the current passing through backup relay OCR1 falls below I_F^{min}, the coordination among the protection relays depicted in Figure 1 is compromised; OCR1 fails to act as backup protection and is likely to function within its overload region instead.

If the EVs are integrated between the OCR1 and OCR2, during a fault, the main relay current decreases while the backup relay current increases. With an increasing penetration level of integrated EVs, their injected currents into the fault location increase. Consequently, the current through the main relay OCR2 decreases further and the current through the backup relay OCR1 increases more. At certain levels of EV integration, protection coordination can be jeopardized if the backup relay's characteristic curve is adjusted such that an increase in current beyond I_F^{max} shortens the time interval between the two relays. Also, considering that due to lowered sensitivity, the main relay may refuse to operate after an EV is integrated, and with an increment of the current through the backup relay, this relay operates as sympathetic tripping and the protection system fails to meet the requirement of selectivity. False tripping can result in an unnecessary outage of a healthy distribution feeder.

3. Protection Miscoordination in the Presence of EVs

We consider the system shown in Figure 1 without the EVCSs. A fault occurring downstream of the main protection (at bus C) leads to identical currents flowing through the OCR1 and OCR2, expressed as

$$I_{OCR1} = I_{OCR2} = I_g = \frac{V_g}{Z_T}, \tag{3}$$

where I_g denotes the network's injected fault current, V_g represents the upstream network voltage, and Z_T is the total impedance path from the upstream grid to the fault point. With equal currents through both relays, the backup relay is designed to act after a predetermined CTI if the main relay fails to respond.

The EV charger usually employs an inner loop for current control and an outer loop for power control based on feed-forward compensation and proportional-integral (PI) controller. Thus, the EV charger can be modeled by using a current source associated with the control command [41, 42]. Constrained by the physical properties of the semiconductor switches, when a fault occurs in the distribution system, the permissible current through the converter of an EV charger should be limited to the maximum

value for protecting the semiconductor switches from overheating under short-circuit fault conditions. When the amplitude of the controller output current exceeds the maximum value, it will be limited to $I_{\max}$ and the EV charger changes the control mode to the constant power control with the output of active power as the priority. In this condition, the charging current of the EV charger I_{EV} and the measured voltage at the point of connection to the grid are approximately reversed in phase [24, 25]. This study delves into the dynamics of short-circuit currents contributed by EVs to the distribution network via the grid-side converter. The investigation encompasses both DC fast charging and AC slow charging systems, noting that the grid-side converter, its control methodologies, and the resultant short-circuit current characteristics remain consistent across these charging modalities. Consequently, the protection scheme proposed herein is universally applicable to both types of charging infrastructures.

3.1. Integration of EVs Upstream From the Main and Backup Relays. If the EV is integrated upstream from the main and backup relays, the currents through both relays decrease depending on the penetration level of integrated EVs as

$$I_{\mathrm{OCR1}} = I_{\mathrm{OCR2}} = \frac{1}{Z_T}\left[V_g - \sum_{i=1}^{m} I_{\mathrm{EV}_i}\left(Z_1 + \sum_{j=1}^{n} Z_j\right)\right], \quad (4)$$

where I_{EV_i} is the current of i th EV integrated upstream from two protection relays, Z_1 is the impedance between the farthest integrated EV from the backup relay and the upstream network, and Z_j is the impedance between two consecutive integrated EVs. With the integration of EVs, the operating dynamics of both main and backup OCRs change, notably a decrease in their currents leading to extended operating times and longer intervals between the activations of these two relays. Such a decrease in current levels, if maintained within the bounds of $I_F^{\min}$ and $I_F^{\max}$, can enhance the protective coordination during faults by ensuring a safer operational window for the backup relay. However, (4) shows that a higher EV penetration level further diminishes the currents through both the main and backup relays, delaying the backup relay's action beyond the originally coordinated time, possibly even surpassing the thermal limits of the network's conductors.

Figure 2 shows that for the fault current I_g, OCR2 is expected to act at time t_{OCR2}. In case of its failure, OCR1 would ideally kick in after a CTI, operating at t_{OCR1} without breaching the thermal constraints of the conductors. Yet, with 100% EV penetration upstream of these relays, the backup relay's current reduces down to $I_F^{\min}$. Given this scenario, if the network encounters $I_F^{\max}$ current, the allowable fault clearance time is capped by t_{thermal}. In other words, if the network current is $I_F^{\max}$, the fault clearing time should be smaller than t_{thermal}. However, with the actual current at OCR1 being $I_F^{\min}$, its operational time extends to $t_{\mathrm{OCR1}}{}'$, violating the conductor's thermal limit. Typically, the longest permissible operation time for a backup relay in distribution networks is set at 1000 ms, implying that the operational curves for both main and backup protections must sit beneath the thermal limit curve, as shown in Figure 2. Therefore, by considering the highest level of EV integration as a worst-case scenario and reducing the backup relay's I_{OCR1} to $I_F^{\min}$, it is imperative to adjust the OCR1 relay's operation time $t_{\mathrm{OCR1}}{}'$ back within thermal limits, t_{thermal}, below the I^2t curve. This adjustment necessitates limiting the EVs' current injection into the fault, thus ensuring the backup relay's current reduction is effectively managed. Consequently, the operating point of the backup relay, altered by the EVs' presence, is readjusted, preserving the protection coordination.

3.2. Integration of EVs Between the Main and Backup Relays. In the case of EVs integrated between the main and backup protections and a fault at downstream of OCR2, the currents through the backup and main relays are expressed as

$$I_{\mathrm{OCR1}} = \frac{1}{Z_T}\left[V_g + \sum_{i=1}^{m} I_{\mathrm{EV}_i}\left(Z_F + Z_2 + \sum_{j=1}^{n} Z_j\right)\right], \quad (5)$$

$$I_{\mathrm{OCR2}} = \frac{1}{Z_T}\left[V_g - \sum_{i=1}^{m} I_{\mathrm{EV}_i}\left(Z_T - \left(Z_F + Z_2 + \sum_{j=1}^{n} Z_j\right)\right)\right], \quad (6)$$

where Z_F is the fault resistance plus the impedance between OCR2 and fault location and Z_2 is the impedance between integrated EV near OCR2 and this relay. By integrating EVs closer to OCR2, a significant dynamic shift occurs in the distribution system's protection operation due to changes in fault currents. Specifically, equations (5) and (6) show that as the penetration level of EV increases, the backup relay experiences an increase in current, while the main relay observes a decrease. This shift results in the main protection delaying its operation beyond its originally set time, potentially exceeding the network conductors' thermal limit if the backup protection fails to activate. In such scenarios, traditional protection settings, which do not account for the varying current contributions from integrated EVs, may lead to decreased sensitivity of the main relay, risking its failure to trigger. On the other hand, increasing the current through the backup relay leads to a reduction of its operation time and false tripping, that is, selectivity is not satisfied. Thus, to avoid failure and guarantee the selectivity of the current protection, restoration of protection coordination by adjusting the injected EV charger current can be implemented.

3.3. Simultaneous Integration of EVs Between and Upstream From the Main and Backup Relays. The integrated EVs may be simultaneously integrated between and upstream from the main and backup relays. If EV1 is integrated into the upstream of the backup relay and EV2 is integrated between the main and backup relays, then by ignoring Z_F in (5), the OCR1 current is calculated as

$$I_{\mathrm{OCR1}} = I_g - \left(\frac{Z_1}{Z_T}\right) I_{\mathrm{EV1}} + \left(\frac{Z_2}{Z_T}\right) I_{\mathrm{EV2}}, \tag{7}$$

where I_{EV1} and I_{EV2} are injected fault currents of EV1 and EV2, respectively.

Depending on the location of integrated EVs along the feeder, the current of the backup relay is greater or less than its initial value I_g. If the capacity of Station 1 and Station 2 is the same, $I_{\mathrm{EV1}} = I_{\mathrm{EV2}} = I_{\mathrm{EV}}$, then (7) is simplified as

$$I_{\mathrm{OCR1}} = I_g - \left(\frac{Z_1 - Z_2}{Z_T}\right) I_{\mathrm{EV}}. \tag{8}$$

Equation (8) indicates that in the scenario where EVs are simultaneously integrated between and upstream from the relays, the impact of integrated EVs on the backup relay is less significant compared to when the EVs are integrated between or upstream of the relays. Furthermore, if $Z_1 = Z_2$, the integrated EVs do not impact the OCR1 current. In such a scenario, the OCR1 current equals the current of the upstream network, $I_{\mathrm{OCR1}} = I_g$, which is similar to the situation when there are no integrated EVs in the grid. Consequently, this paper exclusively investigates the effects of EVs integrated between relays and those integrated upstream from the backup relay.

4. Proposed Protection Coordination Scheme

As mentioned in Section 3, the presence of integrated EVs can disrupt the protection coordination of the distribution system. Thus, a new scheme is necessary to mitigate the integrated EV effect on the protection system. Figure 3 shows the flowchart of the proposed scheme. The initial step involves conducting a load flow to determine the protection system's initial settings, the current transformer ratio, and the load current. The analysis then progresses to model a fault scenario in the absence of any integrated EVs to determine the branch fault currents through short-circuit calculations. This information is used to ascertain the relays' operating times based on their currents, allowing for an assessment of the protection system's effectiveness. If the protection system is coordinated, the number of integrated EVs is gradually increased in proportion to the rising penetration level of EVs (up to a maximum of 100%). However, once protection coordination is lost at a specified penetration level of EVs, coordination restoration is undertaken using the scheme proposed in the "Coordination Restoration" section of Figure 3. This section is implemented based on an EV charger control system using the CCL strategy, which will be elaborated subsequently. It should be noted that calculations for the proposed coordination restoration scheme are conducted offline. In other words, before network operation, the proposed scheme must be executed for various locations of integrated EVs in the network, and subsequently, the modified settings are calculated.

As mentioned above, the maximum injected current of the EVCS converter during a fault condition should be limited to protect the semiconductor switches from overheating [43]. The limited current of the EV charger during a fault $I_{\mathrm{EV}}^{\mathrm{SC}}$ is calculated as

$$I_{\mathrm{EV}}^{\mathrm{SC}} = k \times I_{\mathrm{EV}}^{\mathrm{rated}}, \tag{9}$$

where $I_{\mathrm{EV}}^{\mathrm{rated}}$ is the rated current of the EV charger and k is the current increment factor which is usually chosen to be two. The aim of the CCL strategy is to restore protection coordination by adjusting the current increment factor. However, selecting this parameter impacts the fault current of the network. Since the integration of EVs in the distribution system has a greater impact on the operating time of backup protection, due to the larger slope of the characteristic curve of the backup relay compared to that of the main relay, limiting the current of EVs close to the backup protection results in the protection coordination restoration; thus, there is no need to limit the current of all integrated EVs. In this condition, by limiting the integrated EVs affecting the backup protection, the effect of their fault current contribution on the main protection is also limited and coordination is restored. Consequently, depending on EV's impact on the protection coordination, the proposed scheme limits the k value solely for those EVCSs that further affect protection coordination.

As mentioned above, the impact of integrated EVs on the current through the main and backup protections depends on their location. According to (4), if the EV is integrated upstream from the backup protection and near this relay, $Z1 \simeq Z_{\mathrm{line1}}$, then the change in current through both relays from its initial value is at its maximum, $I_{\mathrm{OCR1}} = I_{\mathrm{OCR2}} \simeq I_g - -I_{\mathrm{EV}}$. However, if the distance of the integrated EV to the backup relay is substantial and the EV is near the upstream network such that $Z_1 \simeq 0$, then the current through both relays is less affected by the EV integration, $I_{\mathrm{OCR1}} = I_{\mathrm{OCR2}} \simeq I_g$. In addition, as indicated in (5) and (6), if an EV is integrated between two relays and near to the main relay such that $Z_1 \simeq 0$, its effect on the current through the main protection is at its maximum, $I_{\mathrm{OCR2}} \simeq I_g - -I_{\mathrm{EV}}$, while the OCR1 current is close to this current in the scenario without EVs, $I_{\mathrm{OCR1}} \simeq I_g$. If the integrated EV is near the backup relay, $Z_1 \simeq Z_{\mathrm{line2}}$, then its effect on the main protection current is negligible, $I_{\mathrm{OCR2}} \simeq I_g$, and its effect on the backup relay current is at its maximum, $I_{\mathrm{OCR1}} \simeq I_g + I_{\mathrm{EV}}$.

Equations (4) and (5) reveal that the backup protection's current consists of both constant and variable components. The constant component, I_g, is determined by the upstream network's contribution, while the variable component, $I_{\mathrm{OCR1}}^{\mathrm{EV}}$, varies with the penetration level of integrated EVs and their location relative to the relays, either positioned between the two relays or upstream from the backup relay, and this component is expressed as

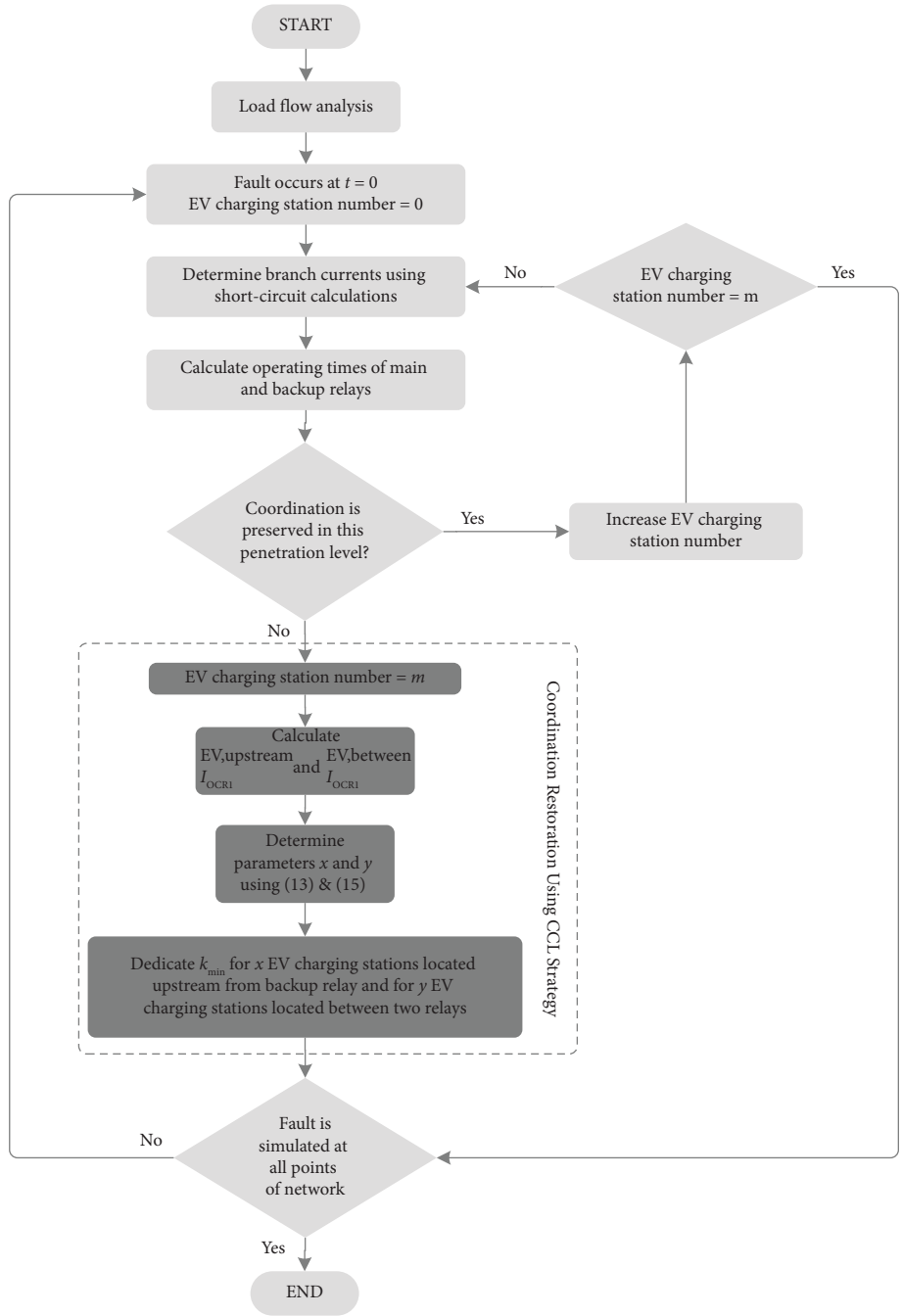

Figure 3: Flowchart of the proposed protection coordination scheme.

$$I_{\mathrm{OCR1}}^{\mathrm{EV}} = \begin{cases} \dfrac{1}{Z_T}\sum_{i=1}^{m} I_{\mathrm{EV}_i}\left(Z_1 + \sum_{j=1}^{n} Z_j\right), & \text{EVs are located upstream from the backup relay,} \\ -\dfrac{1}{Z_T}\sum_{i=1}^{m} I_{\mathrm{EV}_i}\left(Z_F + Z_2 + \sum_{j=1}^{n} Z_j\right), & \text{EVs are located between two relays.} \end{cases} \tag{10}$$

Thus, the backup relay current is $I_{\mathrm{OCR1}} = I_g - -I_{\mathrm{OCR1}}^{\mathrm{EV}}$. By controlling $I_{\mathrm{OCR1}}^{\mathrm{EV}}$, the deviation of the OCR1 current from its initial value can be kept within an allowable range. Maintaining the change in I_{OCR1} within its allowable limit preserves the backup protection coordination. As shown in Figure 4, a current limit for the backup relay to preserve

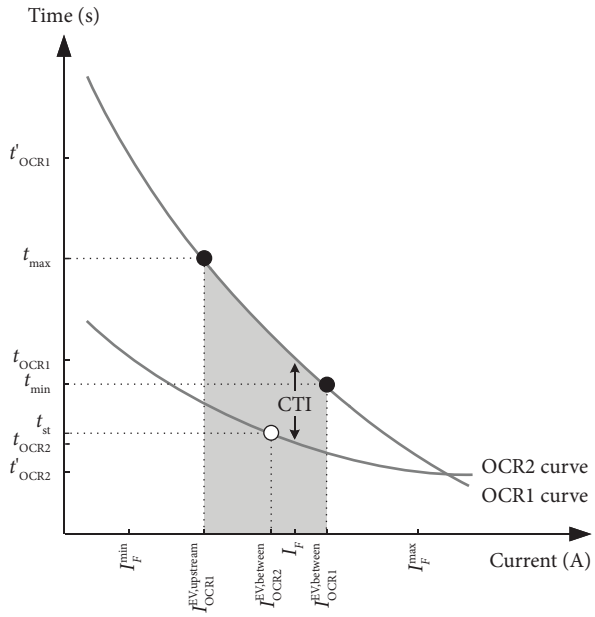

Figure 4: Protection coordination restoration by determination of permissible limit for injected current of EV charger.

protection coordination can be determined by controlling the EV charger current based on the specified time range for the backup relay t_{min} and t_{max}. For this purpose, the maximum penetration level of the integrated EVs is considered. Different methods should be adopted depending on the location of the integrated EVs (whether situated between the two relays or upstream from the backup relay).

4.1. Presence of EVs at Upstream From Backup Protection. In the scenario where the penetration level reaches 100%, ensuring that the backup relay OCR1's operating time falls below the I^2t curve guarantees the preservation of protection coordination for all levels of EV integration. Hence, in situations where EV integration is at its peak, the operating time for the backup relay is set to t_{max}. The current through OCR1 for this highest level of EV integration is determined by applying (4). Following this, the operating time for the backup relay aligns with t_{max}, and as a result, the current through the backup relay, in alignment with the IEC 60255 standard [44], is computed accordingly as

$$I_{OCR1} = I_{base} \times \sqrt[P]{1 + \frac{A \times TMS}{t_{max}}}, \tag{11}$$

where TMS is the time multiplier setting and I_{base} is the relay plug setting current. A and P are constant parameters and they determine the slope of the protection characteristic curve. Since the proposed scheme for restoring the protection coordination for all EVCS arrangements is adjusted once, I_{base}, A, P, and TMS are considered constant and I_{OCR1} is determined based on the operating time t_{max}.

The adjusted current for the backup relay, which ensures preserved protection coordination, is recalculated using (11). Thus, the term of OCR1 current which is affected by the penetration level of integrated EVs is calculated as follows, resulting in an increase from its initial value:

$$I_{OCR1}^{EV,upstream} = I_g - I_{OCR1}. \tag{12}$$

This current increment is strategically allocated based on the geographical placement of EVs and their consequential effect on the backup relay's current. The locations of EVCSs are divided into two parts: those with less impact and those with more impact on the protection system. EVCSs installed in locations that have less impact are allowed to deliver their maximum permissible fault current ($k_{max} = 2$). However, the current increment factor for EVCSs that have a further effect on the backup relay current is decreased to the minimum value of the current increment factor k_{min}.

Using (10), the currents of these two parts are expressed as

$$\begin{aligned} I_{OCR1}^{EV,upsteam} &= I_{OCR1}^{EV,upsteam\,(more)} + I_{OCR1}^{EV,upsteam\,(less)} \\ &= \frac{1}{Z_T}\sum_{i=1}^{x}\left[k_{min} \times I_{EV_i}\left(Z_1 + \sum_{j=1}^{n} Z_j\right)\right] \\ &\quad + \frac{1}{Z_T}\sum_{i=x+1}^{m}\left[k_{max} \times I_{EV_i}\left(Z_1 + \sum_{j=1}^{n} Z_j\right)\right], \end{aligned} \tag{13}$$

where x is the number of those EVCSs whose currents should be more limited based on the proposed scheme. Using (12), the parameter x is calculated by solving (13). Finally, the current increment factor for those EVCSs is set to k_{min}.

4.2. Presence of EVs Between Two Protection Relays. OCR1 current is determined using (5) for the highest penetration level of integrated EVs. The operating time of the backup relay is equal to t_{min} and consequently, the backup relay current is calculated as

$$I_{OCR1} = I_{base} \times \sqrt[P]{1 + \frac{A \times TMS}{t_{min}}}. \tag{14}$$

Using (14), the variable term of the backup relay current is calculated as

$$\begin{aligned} I_{OCR1}^{EV,between} &= I_g - I_{OCR1} = I_{OCR1}^{EV,between\,(more)} + I_{OCR1}^{EV,between\,(less)} \\ &= -\frac{1}{Z_T}\sum_{i=1}^{y}\left[k_{min} \times I_{EV_i}\left(Z_F + Z_2 + \sum_{j=1}^{n} Z_j\right)\right] \\ &\quad - \frac{1}{Z_T}\sum_{i=y+1}^{m}\left[k_{max} \times I_{EV_i}\left(Z_F + Z_2 + \sum_{j=1}^{n} Z_j\right)\right], \end{aligned} \tag{15}$$

where y is the number of EVCSs located between two relays that further affect I_{OCR1}. By calculating y, the current increment factor for these EVCSs is set to k_{min}.

Also, the current through the main relay which is affected by applying k_{min} to effective EVCSs located between the two relays is determined as follows which is more than its previous value:

$$I_{\mathrm{OCR2}} = I_g - I_{\mathrm{OCR2}}^{\mathrm{EV,between}} = \frac{1}{Z_T} \cdot \left[V_g - \left\{ \sum_{i=1}^{y} \left[k_{\min} \times I_{\mathrm{EV}_i} \left(Z_T - \left(Z_F + Z_2 + \sum_{j=1}^{n} Z_j \right) \right) \right] + \sum_{i=y+1}^{m} \left[k_{\max} \times I_{\mathrm{EV}_i} \left(Z_T - \left(Z_F + Z_2 + \sum_{j=1}^{n} Z_j \right) \right) \right] \right\} \right]. \tag{16}$$

Due to the increment of I_{OCR2} in (16), the operating time of the main relay is reduced to t_{st}, as shown in Figure 4. It preserves the operation sensitivity threshold of this relay, ensuring that protection coordination is not lost. The flowchart of the proposed scheme for restoring protection coordination by controlling the charger output current is shown in the "Coordination Restoration Using CCL Strategy" section of Figure 3.

5. Performance Evaluation

To assess the proposed protection coordination scheme's effectiveness, a segment of the Isfahan city electrical distribution system in Iran is analyzed, incorporating EVs at various points. The system, depicted in Figure 5, is represented in a single-line diagram and modeled within the ETAP software environment. This network features two 20 kV overhead three-wire systems arranged radially, predominantly serving residential loads connected via 20 kV/400 V transformers.

Feeder one is protected by OCR1 and OCR2, while feeder two is protected by OCR3. The protection zone of each PD is illustrated in Figure 5. During normal operation, the feeders do not connect together. However, an interlock mechanism between Switch S and Circuit breaker CB1 ensures feeder 1's load continuity if CB1 trips due to a nonfault event. In this section, the coordinated operation of OCR1 and OCR2 is initially examined under conventional and proposed schemes. Following this initial assessment, the effectiveness of the proposed scheme is further evaluated in scenarios where feeder two is interconnected with feeder 1 via Switch S, examining how this setup impacts the overall system's protection coordination.

5.1. Case 1: Conventional Protection System. According to the standard protection framework of distribution networks, feeders are protected by OCRs [45] designated as main and backup protections, whereas lateral branches are protected by fuses [46]. A CTI of at least 350 ms is mandated to prevent operational disruptions between two PDs, with the upper limit set at 1000 ms to preclude conflicts with the conductors' thermal limit.

In scenarios devoid of EVs, the maximum fault current within OCR2's protection zone reaches 787 A for a three-phase fault at point F. Initial settings dictate OCR2's response time at this current to be 240 ms. If OCR2 fails, OCR1 is designed to act after a CTI of 350 ms, culminating in a total response time of 590 ms.

The introduction of EVs into the system alters fault current based on their penetration rate and positioning. Initially considering a 10% EV integration level, and situating EVs upstream of the backup protection encountering a fault at point F, the currents through both OCR1 and OCR2 diminish uniformly to 743 A. The operation timings for the main and backup relays adjust to 258 ms and 697 ms, respectively, reflective of the fault's location within the protection zones.

Placing EVs between OCR1 and OCR2 varies the fault currents to 832 A and 707 A, respectively, at point F's three-phase fault scenario. Consequently, the main and backup relays' activation times are revised to 272 ms and 516 ms, respectively.

Compared to the EV-free grid, integrating EVs upstream of the backup protection extends the CTI between OCR1 and OCR2, enhancing protection system's efficiency by prolonging the backup relay's operational period. A 10% EV penetration that enhances system performance by accelerating fault clearance should the main relay malfunction. Conversely, when EVs are positioned between the relays, this penetration level increases the main relay's activation time while reducing the backups, speeding up fault clearance.

Elevating EV penetration levels above 10%, especially when EVs are positioned upstream of both relays, elongates both OCR1 and OCR2's response times. Table 2 details the effects of EV integration on the conventional protection scheme's relay timings. Beyond a 70% EV penetration, the backup relay's operation interval surpasses the 1000 ms thermal limit, reaching 1810 ms at 100% penetration, as depicted in the simulation results in Figure 6.

For EV integrations exceeding 10%, the narrowed CTI between OCR1 and OCR2, due to OCR1's reduced response time and OCR2's elongated period, is further constrained. Table 3 illustrates the impact of EVs positioned between the main and backup protections on their operational timings. At a 20% EV penetration, the CTI dips below the minimum limit of 240 ms, with Figure 7 showcasing the conventional protection system's efficacy under these conditions, where a 100% EV penetration minimizes the CTI to merely 30 ms.

5.2. Case 2: Proposed CCL Strategy. The CCL strategy fine-tunes the current increment factor for EVCSs depending on their influence on the protection system. According to (13), for x EVCSs positioned upstream relative to both the main and backup relays and proximate to the backup relay, the current increment factor is adjusted to a minimum value, $k_{\min}$. On the contrary, the current increment factor for the remaining EVCSs is kept at its standard level, $k_{\max} = 2$. When EVCSs are situated between the main relay (OCR1) and the backup relay (OCR2), based on (15), the current increment factor for y EVCSs close to the backup relay is reduced to $k_{\min}$. Meanwhile, the factor for the rest of the

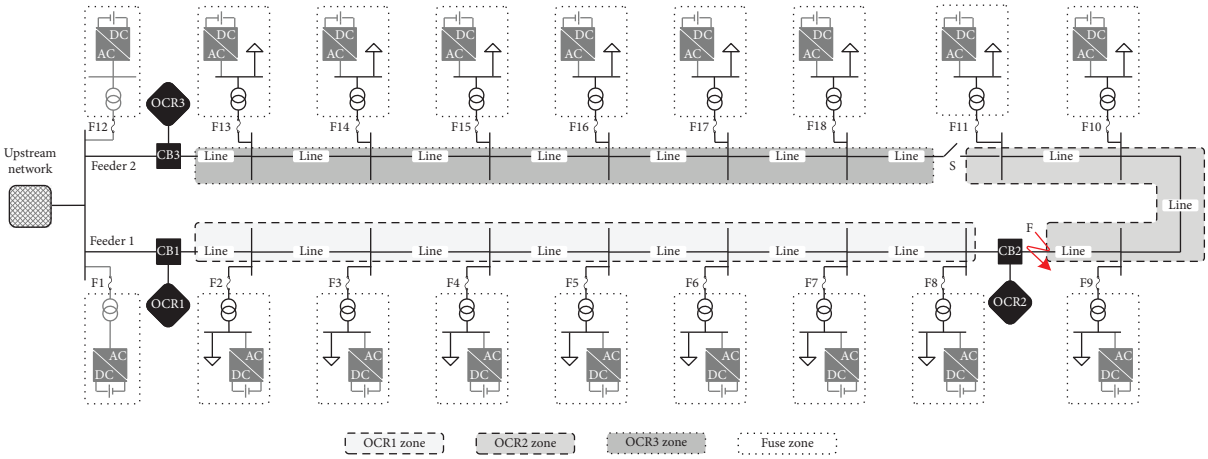

Figure 5: Single-line diagram of the study's test system with integrated EVCSs.

Table 2: Operating time of the study's test system in the presence of EVs integrated upstream from the backup relay.

Grid integration of EV Penetration level (%)	Conventional scheme			CCL strategy
	t_{OCR1} (ms)	t_{OCR2} (ms)	Δt (ms)	t_{OCR1} (ms)
0	590	240	350	590
10	69	258	439	595
20	805	271	534	602
30	920	285	635	609
40	1036	296	740	619
50	1157	306	851	632
60	1283	316	967	661
70	1413	324	1089	687
80	1548	331	1217	716
90	1686	337	1349	748
100	1831	343	1488	776

EVCSs is preserved at $k_{max} = 2$. In the case of the system under study, x and y values are determined to be 2 and 4, respectively, with k_{min} set at 1.2.

The performance of the proposed scheme in cases of EVs integrated upstream and between the relays is presented in Tables 2 and 3, respectively. The implementation of the proposed scheme ensures effective coordination between the main and backup OCRs (OCR1 and OCR2) for all levels of EV integration into the grid, whether through private or public charging stations. Figure 8 verifies that the CCL strategy successfully maintains the current passing through the protection relays within acceptable boundaries, irrespective of the EVs' integration levels and locations.

Specifically, when EVs are connected upstream of the protection relays, a minimum time gap of 200 ms between the operating times of OCR1 and the conductor's thermal limit curve is necessary to guarantee the backup relay's proper functionality. For the highest EV penetration level (100%), the backup relay's permissible operating time is set to 800 ms, with it activating at 776 ms for a fault current of 592.3 A, significantly sooner than the 1831 ms delay observed with the traditional protection system.

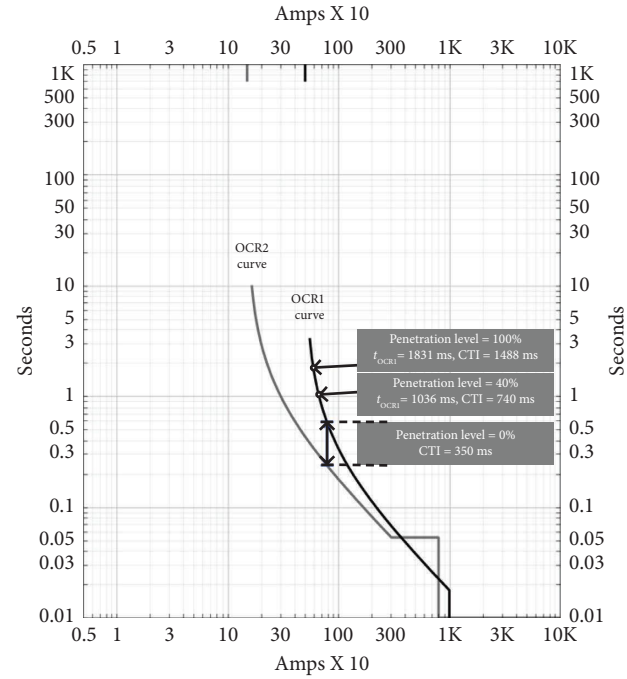

Figure 6: Performance of the conventional protection system; EVs are integrated upstream from the backup relay.

In those cases where EVs are integrated between the protection relays, the current through the main relay is determined considering the penetration level of 100%. Subsequently, the operating time of OCR1 is calculated. To restore coordination, the trip command time of OCR1 is determined by considering the allowable initial time interval CTI from the operating time of OCR2. In this condition, if the CCL strategy is used, the operating time of the backup relay, t_{min}, increases from 401 to 559 ms for a penetration level of 100%, and protection coordination is restored.

By using the CCL strategy and matching t_{min} and t_{max} points on the OCR1 and OCR2 characteristic curves, protection coordination is preserved between OCR1 and OCR2, as well as between OCR1 and the I^2t curve for all penetration

Table 3: Operating time of the study's test system in the presence of EVs integrated between main and backup relays.

Grid integration of EV Penetration level (%)	Conventional scheme			CCL strategy	
	t_{OCR1} (ms)	t_{OCR2} (ms)	Δt (ms)	t_{OCR1} (ms)	t_{OCR2} (ms)
0	590	240	350	590	240
10	516	272	244	584	244
20	473	296	177	580	247
30	443	313	130	572	250
40	426	324	102	568	252
50	417	336	81	565	254
60	412	346	66	563	256
70	408	354	54	561	257
80	405	361	44	560	258
90	402	367	35	559	258
100	401	371	30	559	258

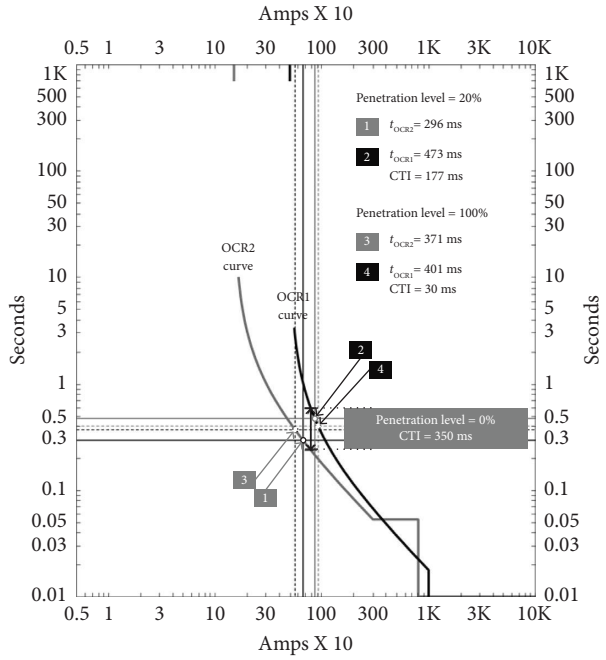

Figure 7: Performance of the conventional protection system; EVs are integrated between main and backup protection relays.

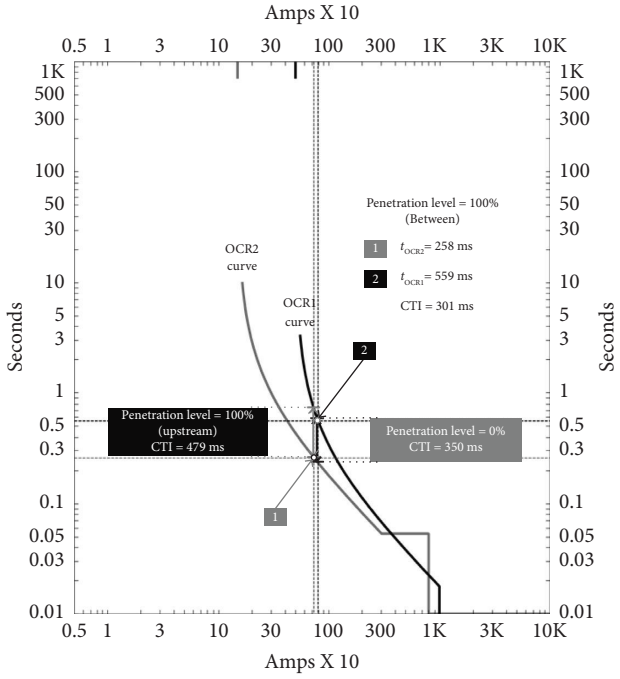

Figure 8: Performance of the proposed CCL strategy in the presence of integrated EVs upstream and between main and backup relays.

levels and locations of integrated EVs. Even in the absence of EVs, the protection system operates coordinately.

By calculating the current through the backup relay for the maximum penetration level of EVs and using this current, the operating time of the backup relay t_{OCR1} is determined using the conventional equation of the delayed operation part of the OCR characteristic curve in accordance with [44] as

$$t_{OCR1} = \frac{A \times TMS}{\left(I_{OCR1}/I_{base}\right)^{P} - 1}. \quad (17)$$

The ratio of the backup relay current to its plug setting current I_{OCR1}/I_{base} in (17) is defined as the plug setting multiplier (PSM). As mentioned in Section 2, in the absence of EVs, OCR1 and OCR2 coordinately operate in the current range $[I_F^{min} I_F^{max}]$. PSM values for the minimum and maximum fault currents are 1.3326 and 1.8047, respectively. When the traditional protection system is utilized, and the EV penetration level reaches 100%, the resulting PSM values 1.1953 and 1.9013 lie outside the predefined coordination range [1.3326, 1.8047]. However, the CCL strategy corrects this discrepancy, bringing the PSM values [1.3326, 1.8047] within the acceptable coordination range, thus ensuring that the protection scheme remains effective even at full EV penetration. This demonstrates the CCL strategy's capability to adaptively manage protection settings in response to varying levels of EV integration.

5.3. Case 3: High-Impedance Faults (HIFs). When an overhead conductor encounters a high-impedance object or lands on a surface with high impedance, a HIF occurs. This type of fault is characterized by its high fault resistance, leading to relatively low currents being detected by protection relays during the event. This can present a challenge for conventional protection systems, which might not operate effectively due to the low currents, potentially failing to clear the fault promptly and risking damage to the network. According to Table 4, in scenarios where EVs are integrated into the distribution system upstream from both the main and backup relays, the conventional protection system may not suffice during single phase to ground HIFs. When the conventional protection system is used, the thermal limit is violated at penetration levels of 50% and 30% for fault resistances of 15 Ω and 30 Ω, respectively. However, the CCL strategy gives satisfactory results for all penetration levels of EVs. Employing the CCL strategy significantly enhances the system's response to such HIFs, even with varying levels of EV integration. Despite the inherent challenge of reduced relay currents during HIFs, the CCL strategy effectively maintains coordination between the main and backup relays. It ensures that, despite the increase in relay operating times due to lower fault currents, the system's protection coordination is preserved without exceeding the thermal limits of the conductors. This adaptability of the CCL strategy to maintain protective coordination under HIF conditions, regardless of the EV penetration level, showcases its value in modern electrical distribution systems. It enhances the reliability and safety of the network by ensuring that even under challenging fault scenarios, the protection system operates within its designed parameters, safeguarding both the infrastructure and the consumers it serves.

5.4. Case 4: Network Topology Change. When the Switch S is activated, linking Feeder 2 to Feeder 1 while Circuit breaker CB1 is disengaged, the operational dynamics of the system shift, designating OCR2 as the main relay and OCR3 as its backup relay. In the absence of EVs, the coordination between the main and backup relays is efficiently maintained with operating times of 240 ms and 590 ms, respectively, achieving the intended CTI of 350 ms. When the penetration level of integrated EVs upstream from the relays increases up to 40%, OCR3 operates at 1085 ms which leads to miscoordination of relays. In addition, the coordination of relays is lost in the penetration level of 20% when the EVs are integrated between relays.

The comparative analysis presented in Table 5 highlights the operational impacts on the main and backup relays' operating times due to EV integration, both upstream and between the relays. These insights underscore the efficacy of the proposed CCL strategy in addressing coordination disruptions caused by EV integration. By implementing the CCL strategy, the system regains its designed relay coordination for all studied EV penetration levels, ensuring reliable protection operation and enhancing the overall stability and safety of the electrical distribution network.

6. Sensitivity Analysis

Sensitivity analysis plays an important role in coordination studies. In cases where the sensitivity requirements for the backup relays are not met, it leads to longer operating times. The sensitivity analysis examines the sensitivity threshold of the backup relay to guarantee that the operation of this relay for the minimum fault current occurred at the end of the protection zone of its main relay, as [29]

$$\text{Sensitivity} = \frac{I_{\text{OCR1}}^{\text{SC}}}{k' I_{\text{Load}}^{\max}}, \tag{18}$$

where $I_{\text{OCR1}}^{\text{SC}}$ is the current that the backup relay senses for the minimum fault simulated at the far end of its main relay protection zone, k' is the temporal overload factor of the backup relay, and $I_{\text{Load}}^{\max}$ is the maximum load current of the backup relay.

According to (18), it is found that the sensitivity threshold of the backup relay for the minimum short-circuit current without EV is 1.3. This value is very important as a comparative reference for sensitivity analysis in this study. Integration of EVs upstream of both protections violates the minimum sensitivity required in the backup relay. As specified in (4), this violation occurs due to the reduction of the fault current in the presence of the EV and leads to a significant time delay for the backup relay in clearing the fault. When the conventional protection system is used, as the penetration level of EV increases, the sensitivity of the backup relay reaches the minimum threshold of 0.9468; this relay operates in the overload region and the thermal limit of the network conductor is violated. The reduction in the sensitivity of the backup relay with the increase of EV penetration level is shown in Figure 9(a). At the EV penetration level of 46%, the backup relay sensitivity falls below the threshold value of 1.3, potentially leading to a tripping delay.

Increasing the penetration level of EV in the case of its integration between both protective relays, which according to (5) leads to an increase in the current passing through the backup relay, increases the sensitivity of this relay so that it reaches 1.9013 in the worst case and exceeds the coordination threshold of 1.8047 in the condition of the maximum short-circuit current obtained from (18). Increasing the sensitivity of the backup relay leads to a decrease in CTI, and with a violation of selectivity, it causes the backup relay to operate instead of the main relay. It can be seen in Figure 9(b) that the sensitivity of the backup relay increases by increasing the penetration level of integrated EVs between both relays, and the selectivity is compromised by decreasing the CTI between both protections. In this scenario, early activation of the backup protection system before the main protection ensures the loss of coordination. For 33% EV penetration level, the backup relay sensitivity exceeds the acceptable limit of 1.8278, as shown in Figure 9(b).

Figure 9 verifies the increased sensitivity achieved through the implementation of the proposed CCL strategy. This strategy ensures that the sensitivity of the backup relay remains within the permissible range [1.3, 1.8047] in

Table 4: Operating time of the study's test system in the presence of EVs integrated upstream from a backup relay in the case of a HIF.

Fault resistance	Grid integration of EV Penetration level (%)	Conventional scheme			CCL strategy
		t_{OCR1} (ms)	t_{OCR2} (ms)	Δt (ms)	t_{OCR1} (ms)
15 Ω	0	602	252	350	602
	10	712	276	436	616
	20	847	296	551	633
	30	1008	313	695	651
	40	1219	329	890	671
	50	1481	341	1140	694
	60	1859	352	1507	718
	70	2342	361	1981	747
	80	3031	371	2660	777
	90	3794	379	3415	809
	100	4676	386	4290	840
30 Ω	0	611	261	350	611
	10	826	297	529	624
	20	1089	324	765	639
	30	1394	347	1047	651
	40	1793	368	1425	671
	50	2152	385	1767	703
	60	2613	397	2216	736
	70	3183	407	2776	773
	80	3831	416	3415	813
	90	4646	423	4223	856
	100	5631	429	5202	902

Table 5: Operating time of the study's test system in the case of network topology change.

Installation location	Grid integration of EV Penetration level (%)	Conventional scheme			CCL strategy
		t_{OCR3} (ms)	t_{OCR2} (ms)	Δt (ms)	t_{OCR3} (ms)
Upstream from the relays	0	590	240	350	590
	10	706	263	443	601
	20	825	279	546	609
	30	954	293	661	621
	40	1085	306	779	635
	50	1224	318	906	662
	60	1374	327	1047	693
	70	1536	336	1200	721
	80	1712	344	1368	755
	90	1894	351	1543	774
	100	2085	357	1728	794
Between two relays	0	590	240	350	590
	10	539	261	278	585
	20	504	278	226	581
	30	484	290	194	575
	40	469	299	170	573
	50	459	310	149	571
	60	453	320	143	568
	70	449	328	121	566
	80	446	334	112	565
	90	444	338	106	564
	100	443	339	104	564

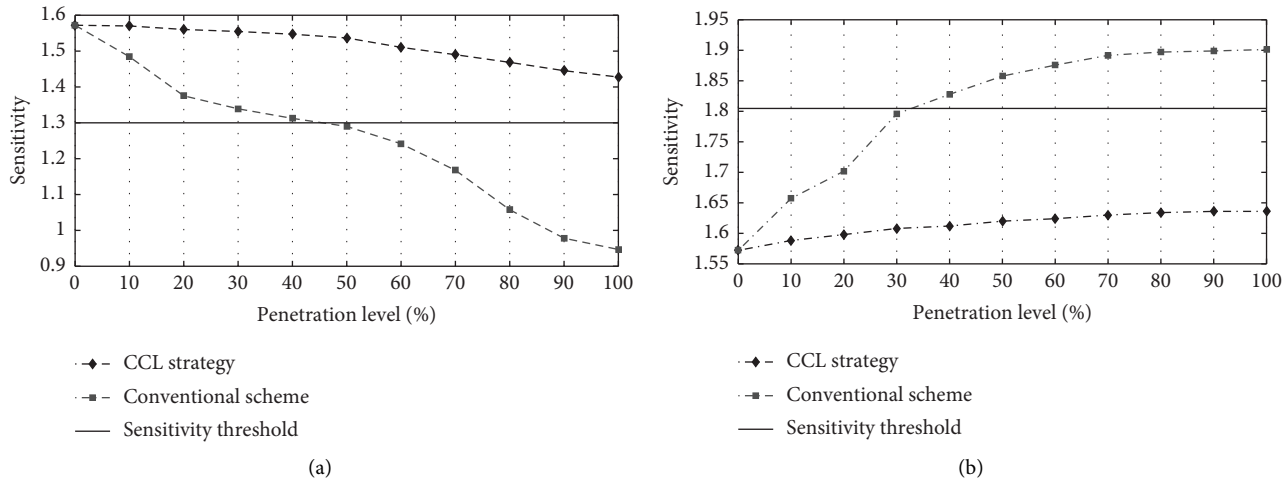

Figure 9: The sensitivity of the backup relay: (a) EVs are integrated upstream from the backup relay and (b) EVs are integrated between the main and backup relays.

Table A1: Parameters of the study's test system.

Parameter	Specification
Length of feeder	30 km
Type of feeder	Headway type and not transposed-radial
Conductor size	MV line: 120 mm^2; LV line: cable $4 \times 50 + 25$ mm^2
Line shape	Horizontal and distance between lines: 70, 140, and 70 cm
Nominal voltage	MV: 20 kV_{LL}, LV: 400 V_{LL}, 3ph + N + PE
Legs altitude	9 m
Transformer	630 kVA, Δ/Y-grounded, 20 kV/0.4 kV
Short-circuit power of the main substation	500 MVA
EV rectifier	40 ~ 200 kVA and with battery
Load unit power	200 kVA

different locations and penetration levels of EVs integration. The significant advantages of the proposed scheme are meeting selectivity criteria and increasing the sensitivity of backup protection.

7. Conclusion

This paper is motivated by the impact of EV integration on the performance of the protection system of distribution networks. The study aims to preserve the protection coordination of radial distribution systems in the presence of integrated EVs with various penetration levels and locations. It was found that the effect of EV grid integration during a fault condition is significantly different from normal operation, leading to disruption of protection system performance. Protection coordination is restored by limiting the injected current of EVCSs during fault conditions. It prevents the miscoordination of the main and backup protections and the violation of the thermal limit of the network conductors by guaranteeing the operation of the relays in the safe protection interval. The study of the Isfahan distribution system demonstrates that by identifying EVCSs that greatly impact the protection system and limit their injected currents during faults, the proposed CCL strategy enhances the performance of the protection system without imposing limitations on the injected current of other chargers. In addition, despite the inherent challenge of reduced relay currents during HIFs, the adaptability of the proposed CCL strategy to preserve the protection coordination under HIF conditions regardless of the EV penetration level was verified. Also, in the case of a change in the topology of the radial distribution system, the proposed strategy was able to preserve the protection coordination. Furthermore, the proposed strategy ensures that the sensitivity of the backup protection remains above the minimum coordination sensitivity threshold by maintaining the CTI within the permissible range. The proposed scheme does not require communication links, their calculations can be performed offline, and there is no need for new investment including replacement and installation of new protective devices, or designing new online control functions. The procedure can be applied to different types of old and new programmable relays. As the adoption of EVs continues to rise, the insights and findings presented in this paper can serve as valuable guidelines for utilities and system operators in ensuring the reliable and efficient protection of distribution systems in the electrified transportation era.

Appendix

The parameters of the study system are detailed in Table A1.

As mentioned in Section 5, in the scenario where Switch S is open in Figure 5, OCR2 will serve as the main protection, and OCR1 will act as the backup protection. If Switch S is closed and CB1 opens, then OCR2 will function as the main protection, and OCR3 will serve as the backup protection. Throughout the simulation, the operating equation for relays OCR1, OCR2, and OCR3 with a very inverse curve is determined using the delayed operating equation according to IEC60255 standard as [44]

$$t_{\mathrm{OCR}} = \frac{13.5 \times \mathrm{TMS}}{\left(I_{\mathrm{SC}}/I_{\mathrm{base}}\right) - 1}. \tag{A.1}$$

In both operational states of the study distribution system (with Switch S open and closed) and in the absence of EVs, the maximum and minimum short-circuit currents at the closest bus to and farthest bus from the main relay are initially determined. Subsequently, the minimum operating time for the main relay is calculated based on the minimum TMS value. Moreover, considering the standard CTI range of 300–400 ms, both the operating time and TMS for the backup relay are determined at both maximum and minimum short-circuit current limits. The lower TMS value is designated as the backup protection TMS. For the scenario where CB1 is closed and the maneuver Switch S is open, by determining the TMS values of OCR1, OCR2, and OCR3 which are equal to 0.075, 0.05, and 0.125, respectively, CTI between OCR1 and OCR2 is calculated as

$$\mathrm{CTI} = \frac{13.5 \times 0.075}{(787/290) - 1} - \frac{13.5 \times 0.05}{(787/206.5) - 1} = 350\mathrm{ms}. \tag{A.2}$$

Data Availability Statement

No underlying data were collected or produced in this study.

Conflicts of Interest

The authors declare no conflicts of interest.

Funding

This research received no specific grant from any funding agency in the public, commercial, or not-for-profit sectors.

References

[1] International, "Electric vehicles".

[2] Ren, "Renewables 2023 global status report: Renewables in energy demand".

[3] F. Justin, G. Peter, A. A. Stonier, and V. Ganji, "Power Quality Improvement for Vehicle-To-Grid and Grid-To-Vehicle Technology in a Microgrid," *International Transactions on Electrical Energy Systems* 2022 (2022): 1–17, https://doi.org/10.1155/2022/2409188.

[4] H. Das, M. Rahman, S. Li, and C. Tan, "Electric Vehicles Standards, Charging Infrastructure, and Impact on Grid Integration: A Technological Review," *Renewable and Sustainable Energy Reviews* 120 (2020): 109618, https://doi.org/10.1016/j.rser.2019.109618.

[5] Q. Wu, *Grid Integration of Electric Vehicles in Open Electricity Markets* (John Wiley & Sons, 2013).

[6] T. Unterluggauer, J. Rich, P. B. Andersen, and S. Hashemi, "Electric Vehicle Charging Infrastructure Planning for Integrated Transportation and Power Distribution Networks: A Review," *eTransportation* 12 (2022): 100163, https://doi.org/10.1016/j.etran.2022.100163.

[7] E. L. Karfopoulos and N. D. Hatziargyriou, "Distributed Coordination of Electric Vehicles Providing V2G Services," *IEEE Transactions on Power Systems* 31, no. 1 (2016): 329–338, https://doi.org/10.1109/tpwrs.2015.2395723.

[8] S. Wu, "An Adaptive Limited Wide Area Differential Protection for Power Grid With Micro-sources," *Protection and Control of Modern Power Systems* 2, no. 1 (2017): 21–29, https://doi.org/10.1186/s41601-017-0052-2.

[9] K. Mahmud and G. E. Town, "A Review of Computer Tools for Modeling Electric Vehicle Energy Requirements and Their Impact on Power Distribution Networks," *Applied Energy* 172 (2016): 337–359, https://doi.org/10.1016/j.apenergy.2016.03.100.

[10] N. Rajaei, M. H. Ahmed, M. M. A. Salama, and R. K. Varma, "Fault Current Management Using Inverter-Based Distributed Generators in Smart Grids," *IEEE Transactions on Smart Grid* 5, no. 5 (2014): 2183–2193, https://doi.org/10.1109/tsg.2014.2327167.

[11] C. Gong, L. Ma, B. Zhang, et al., "Research on Influence and Resolution of the Relay Protections with Electric Vehicle Charging Station Integrating into Distribution Network," *International Journal of Hydrogen Energy* 42, no. 29 (2017): 18747–18753, https://doi.org/10.1016/j.ijhydene.2017.04.181.

[12] V. R. Pandi, H. H. Zeineldin, and W. Xiao, "Determining Optimal Location and Size of Distributed Generation Resources Considering Harmonic and Protection Coordination Limits," *IEEE Transactions on Power Systems* 28, no. 2 (2013): 1245–1254, https://doi.org/10.1109/tpwrs.2012.2209687.

[13] W. Sheng, S. Zhao, X. Song, and X. Meng, "Maximum Penetration Level of Distributed Generation in Consideration of Voltage Fluctuations Based on Multi-Resolution Model," *IET Generation, Transmission & Distribution* 9, no. 3 (2015): 241–248, https://doi.org/10.1049/iet-gtd.2013.0883.

[14] S. F. Zarei and S. Khankalantary, "Protection of Active Distribution Networks with Conventional and Inverter-Based Distributed Generators," *International Journal of Electrical Power & Energy Systems* 129 (2021): 106746, https://doi.org/10.1016/j.ijepes.2020.106746.

[15] A. M. Al-Sabounchi, J. Gow, and M. Al-Akaidi, "Optimal Sizing and Location of Large Pv Plants on Radial Distribution Feeders for Minimum Line Losses," in *4th International Conference on Electric Power and Energy Conversion Systems (EPECS), Sharjah, United Arab Emirates* (March 2015).

[16] Z. Wang, B. Chen, J. Wang, J. Kim, and M. M. Begovic, "Robust Optimization Based Optimal DG Placement in Microgrids," *IEEE Transactions on Smart Grid* 5, no. 5 (2014): 2173–2182, https://doi.org/10.1109/tsg.2014.2321748.

[17] D. K. Khatod, V. Pant, and J. Sharma, "Evolutionary Programming Based Optimal Placement of Renewable Distributed Generators," *IEEE Transactions on Power Systems* 28, no. 2 (2013): 683–695, https://doi.org/10.1109/tpwrs.2012.2211044.

[18] S. Beheshtaein, R. Cuzner, M. Savaghebi, and J. M. Guerrero, "Review on Microgrids Protection," *IET Generation, Transmission & Distribution* 13, no. 6 (2019): 743–759, https://doi.org/10.1049/iet-gtd.2018.5212.

[19] K. El-Arroudi and G. Joós, "Performance of Interconnection Protection Based on Distance Relaying for Wind Power Distributed Generation," *IEEE Transactions on Power Delivery* 33, no. 2 (2018): 620–629, https://doi.org/10.1109/tpwrd.2017.2693292.

[20] T. S. Aghdam, H. Kazemi Karegar, and H. H. Zeineldin, "Variable Tripping Time Differential Protection for Microgrids Considering DG Stability," *IEEE Transactions on Smart Grid* 10, no. 3 (2019): 2407–2415, https://doi.org/10.1109/tsg.2018.2797367.

[21] A. S. Noghabi, H. R. Mashhadi, and J. Sadeh, "Optimal Coordination of Directional Overcurrent Relays Considering Different Network Topologies Using Interval Linear Programming," *IEEE Transactions on Power Delivery* 25, no. 3 (2010): 1348–1354, https://doi.org/10.1109/tpwrd.2010.2041560.

[22] G. Kaur, A. Prakash, and K. U. Rao, "A Critical Review of Microgrid Adaptive Protection Techniques with Distributed Generation," *Renewable Energy Focus* 39 (2021): 99–109, https://doi.org/10.1016/j.ref.2021.07.005.

[23] M. Uzair, L. Li, M. Eskandari, J. Hossain, and J. G. Zhu, "Challenges, Advances and Future Trends in Ac Microgrid Protection: With a Focus on Intelligent Learning Methods," *Renewable and Sustainable Energy Reviews* 178 (2023): 113228, https://doi.org/10.1016/j.rser.2023.113228.

[24] F. Coffele, C. Booth, and A. Dyśko, "An Adaptive Overcurrent Protection Scheme for Distribution Networks," *IEEE Transactions on Power Delivery* 30, no. 2 (2015): 561–568, https://doi.org/10.1109/tpwrd.2013.2294879.

[25] E. C. Piesciorovsky and N. N. Schulz, "Fuse Relay Adaptive Overcurrent Protection Scheme for Microgrid With Distributed Generators," *IET Generation, Transmission & Distribution* 11, no. 2 (January 2017): 540–549, https://doi.org/10.1049/iet-gtd.2016.1144.

[26] S. Shen, D. Lin, H. Wang, et al., "An Adaptive Protection Scheme for Distribution Systems With Dgs Based on Optimized Thevenin Equivalent Parameters Estimation," *IEEE Transactions on Power Delivery* 32, no. 1 (2017): 411–419, https://doi.org/10.1109/tpwrd.2015.2506155.

[27] H. Wan, K. K. Li, and K. P. Wong, "An Adaptive Multiagent Approach to Protection Relay Coordination With Distributed Generators in Industrial Power Distribution System," *IEEE Transactions on Industry Applications* 46, no. 5 (2010): 2118–2124, https://doi.org/10.1109/tia.2010.2059492.

[28] E. Sortomme, S. S. Venkata, and J. Mitra, "Microgrid Protection Using Communication-Assisted Digital Relays," *IEEE Transactions on Power Delivery* 25, no. 4 (2010): 2789–2796, https://doi.org/10.1109/tpwrd.2009.2035810.

[29] M. Y. Shih, A. Conde, Z. Leonowicz, and L. Martirano, "An Adaptive Overcurrent Coordination Scheme to Improve Relay Sensitivity and Overcome Drawbacks Due to Distributed Generation in Smart Grids," *IEEE Transactions on Industry Applications* 53, no. 6 (2017): 5217–5228, https://doi.org/10.1109/tia.2017.2717880.

[30] E. Abbaspour, B. Fani, I. Sadeghkhani, and H. H. Alhelou, "Multi-agent System-Based Hierarchical Protection Scheme for Distribution Networks with High Penetration of Electronically-Coupled Dgs," *IEEE Access* 9 (2021): 102 998–103 018, https://doi.org/10.1109/access.2021.3098387.

[31] Z. Shuai, C. Shen, X. Yin, X. Liu, and Z. J. Shen, "Fault Analysis of Inverter-Interfaced Distributed Generators With Different Control Schemes," *IEEE Transactions on Power Delivery* 33, no. 3 (2018): 1223–1235, https://doi.org/10.1109/tpwrd.2017.2717388.

[32] P. A. Cavalcante and M. C. Almeida, "Fault Location Approach for Distribution Systems Based on Modern Monitoring Infrastructure," *IET Generation, Transmission & Distribution* 12, no. 1 (2018): 94–103, https://doi.org/10.1049/iet-gtd.2017.0153.

[33] M. Biswal and S. Biswal, "A Positive-Sequence Current Based Directional Relaying Approach for CCVT Subsidence Transient Condition," *Protection and Control of Modern Power Systems* 2, no. 1 (2017).

[34] H. Lin, K. Sun, Z.-H. Tan, C. Liu, J. M. Guerrero, and J. C. Vasquez, "Adaptive Protection Combined With Machine Learning for Microgrids," *IET Generation, Transmission & Distribution* 13, no. 6 (2019): 770–779, https://doi.org/10.1049/iet-gtd.2018.6230.

[35] Y. Guo and C. Fan, "Research on Relaying Technologies of Distribution Network Including Mass Electric Vehicles," *Power System Protection and Control* 43, no. 8 (2015): 14–20.

[36] H. F. Habib, A. O. Hariri, A. ElSayed, and O. A. Mohammed, "Deployment of Electric Vehicles in an Adaptive Protection Technique for Riding through Cyber Attack Threats in Microgrids," in *IEEE International Conference on Environment and Electrical Engineering and IEEE Industrial and Commercial Power Systems Europe (EEEIC/I&CPS Europe)* (June 2017).

[37] G. Naveen, T. H.-T. Yip, and Y. Xie, "Modeling and Protection of Electric Vehicle Charging Station," in *6th IEEE Power India International Conference (PIICON)* (July 2014).

[38] F. Sanchez-Sutil, J. Hernández, and C. Tobajas, "Overview of Electrical Protection Requirements for Integration of a Smart DC Node with Bidirectional Electric Vehicle Charging Stations into Existing AC and DC Railway Grids," *Electric Power Systems Research* 122 (2015): 104–118, https://doi.org/10.1016/j.epsr.2015.01.003.

[39] B. Fani, H. Bisheh, and I. Sadeghkhani, "Protection Coordination Scheme for Distribution Networks with High Penetration of Photovoltaic Generators," *IET Generation, Transmission & Distribution* 12, no. 8 (2018): 1802–1814, https://doi.org/10.1049/iet-gtd.2017.1229.

[40] "IEC Standard for Short-Circuit Currents in Three-phase a.C," *Systems* (2003).

[41] Y.-J. Kim and J. Wang, "Power Hardware-In-The-Loop Simulation Study on Frequency Regulation Through Direct Load Control of Thermal and Electrical Energy Storage Resources," *IEEE Transactions on Smart Grid* 9, no. 4 (2018): 2786–2796, https://doi.org/10.1109/tsg.2016.2620176.

[42] M. A. Haj-ahmed and M. S. Illindala, "The Influence of Inverter-Based DGs and Their Controllers on Distribution Network Protection," *IEEE Transactions on Industry Applications* 50, no. 4 (2014): 2928–2937, https://doi.org/10.1109/tia.2013.2297452.

[43] V. A. Lacerda, R. M. Monaro, R. Peña-Alzola, D. Campos-Gaona, D. V. Coury, and O. Anaya-Lara, "Control-Based Fault Current Limiter for Modular Multilevel Voltage-Source Converters," *International Journal of*

Electrical Power & Energy Systems 118 (2020): 105750, https://doi.org/10.1016/j.ijepes.2019.105750.

[44] "IEC Standard for Single Input Energizing Quantity Measuring Relays With Dependent or Independent Time" (2009).

[45] H. Karimi, G. Shahgholian, B. Fani, I. Sadeghkhani, and M. Moazzami, "A Protection Strategy for Inverter-Interfaced Islanded Microgrids With Looped Configuration," *Electrical Engineering* 101, no. 3 (2019): 1059–1073, https://doi.org/10.1007/s00202-019-00841-6.

[46] F. Hajimohammadi, B. Fani, and I. Sadeghkhani, "Fuse Saving Scheme in Highly Photovoltaic-Integrated Distribution Networks," *International Transactions on Electrical Energy Systems* 30, no. 1 (2020): https://doi.org/10.1002/2050-7038.12148.